Inorganic salts direct the assembly of charged nanoparticles into composite nanoscopic spheres, plates, or needles

Bartosz A. Grzybowski,*[ab] Bartlomiej Kowalczyk,[ab] István Lagzi,[ab] Dawei Wang,[bc] Konstantin V. Tretiakov[d] and David A. Walker[b]

Received 15th April 2012, Accepted 1st June 2012
DOI: 10.1039/c2fd20074k

Oppositely charged, nanoionic nanoparticles can act as "universal surfactants" regulating the growth of ionic microcrystals. This phenomenon derives from a subtle interplay between crystal growth and cooperative electrostatic adsorption of the nanoparticles onto crystal faces. In addition to the electrostatic interactions acting in the system, the nature of salts is also important in the sense that for the same Debye screening length, different salts can mediate formation of markedly different assemblies including supraspheres, nanoneedles, or nanoplates. The method can be further extended to coat non-ionic crystals with appropriately functionalized nanoparticles.

1 Introduction

Self-assembly, SA, of nanoscopic components into "superstructures" of various morphologies is of interest for their size- and shape dependent optical, electronic and magnetic properties[1–3] as well as for the potential applications in the fabrication of magnetic[4] and electronic devices,[5] water remediation,[6] biosensing[7] and energy storage.[8] Such structures have been prepared by a host of methods and include 3D nanoparticle crystals,[9] planar sheets[10] and ribbons,[11] hollow spheres[8] and molecule-like[12,13] and polymer-like[14] assemblies. Preparation of these assemblies entails skilful use and control of nanoscale interactions including van der Waals, steric/entropic, magnetic and electrostatic (for review, see ref. 15). Electrostatic interactions are quite versatile in SA applications since nanoobjects of various material properties can be made charged—to various degrees[16]—by functionalization with charged ligands. We have previously used this strategy to assemble oppositely-charged nanoparticles,[17,18] nanotriangles[19] and nanorods[20] into crystals,[9] heterodimers,[20] "nanomolecules,"[12,13] or dynamic aggregates exhibiting oscillations and/or propagation of chemical waves.[21] Most recently, we have combined the self-assembly of oppositely-charged, (+)/(–) NPs with the growth of microcrystals of inorganic salts ($CaCO_3$, K_2SO_4, Na_2SO_4, and more) as well as charged organic molecules (*e.g.*, (L)-Lysine or vitamin B_5).[24] These compounds were crystallized from

[a]*Department of Chemistry, Department of Chemical and Biological Engineering, Northwestern University, Evanston, Illinois, 60208, USA. E-mail: grzybor@northwestern.edu; Fax: +01 847 491 3024; Tel: +01 847 491 3024*
[b]*Department of Chemical and Biological Engineering, Northwestern University, Evanston, Illinois, 60208, USA. E-mail: grzybor@northwestern.edu; Fax: +01 847 491 3024; Tel: +01 847 491 3024*
[c]*School of Materials Science and Engineering, Northwestern Polytechnical University, Xi'an 710072, China*
[d]*Institute of Molecular Physics, Polish Academy of Sciences, Smoluchowskiego 17, 60-179 Poznan, Poland*

water–DSMO mixtures in the presence of the (+)/(–) nanoparticles. As the crystals grew, the oppositely charged NPs adsorbed onto them in a cooperative fashion to form thin coatings that retarded crystal growth. By increasing the proportion of the NPs to the salt precursors, we were able to favor coating formation *vs.* crystal growth and ultimately control crystal size from tens of microns to ~100 nanometers. In all these experiments, the (+)/(–) NPs acted as a polyvalent "surfactant" effective toward various types of crystallizing materials.

In describing these systems, we found that a continuum description of electrostatic interactions was sufficient—that is, the magnitudes and the ranges of electrostatic forces were regulated by the concentration of inorganic salts present in solution and did not depend on the salt's specific nature. Here, we describe two systems in which the mode of nanoscale electrostatic self-assembly, nESA,[22] is salt specific. We show that depending on the salt's nature and solubility, the same charged nanoparticles can give rise to either supraspheres (using Ni^{2+} salts) or into low symmetry nanoplates or nanoneedles (using Cu^{2+} salts). In the first case, nickel cations facilitate bridging between the assembling NPs; in the latter, particle assembly is templated by the formation of nanoscopic calcium hydroxide seeds. While these examples illustrate the experimental latitude of the nESA method, the general approach can be extended even further, beyond electrostatic and ion-bridging interactions. To outline the opportunities that lie ahead, we provide one illustrative example in which uncharged nanoparticles interact with and coat organic donor–acceptor crystals.

2 Methods

Synthesis and functionalization of AuNPs

(i) AuDDA NPs. Dodecylamine (DDA) coated gold NPs were prepared according to a modified literature procedure[16,17] and had average diameters, 5.0 ± 0.8 nm, as estimated from TEM images of at least 200 NPs from each batch used.

(ii) Ligand exchange on gold NPs. All ultrapure-grade thiols [11-mercaptoundecanoic acid, MUA, and *N*,*N*,*N*-trimethyl(11-mercaptoundecyl)ammonium chloride, TMA] were obtained from ProChimia Surfaces (www.prochimia.com) and used as received. A toluene solution of DDA-capped AuNPs (7 μmol mL^{-1}, 20 mL, 140 μmol) was quenched with 100 mL of methanol to give a black precipitate. The supernatant solution containing excess of capping agent and surfactant was decanted, and the precipitate was washed with methanol (50 mL) and then dissolved in toluene (100 mL) to which a thiol solution (140 μmol) in 10 mL of CH_2Cl_2 was added upon stirring. Thus prepared AuNPs functionalized with thiolate SAMs[23] were allowed to settle down, the mother-liqueur solution was decanted, and the solid was washed with CH_2Cl_2 (3 × 30 mL). The precipitate was then dissolved in 5 mL of methanol by sonication. To introduce negative charges on the AuMUAs, these particles were deprotonated with 25% methanolic solution of NMe_4OH (70 μL, 165 μmol), precipitated with acetone (30 mL), and washed with acetone (2 × 30 mL). The zeta potential of these particles was measured on a Malvern Nano Zeta-Sizer instrument and had an average value of −42.0 ± 4.6 mV. The positively charged AuTMAs were precipitated with ethyl acetate (100 mL) and washed with CH_2Cl_2 and acetone; the zeta potential of these particles was +38.2 ± 3.9. Finally, all the precipitates of thiol-coated AuNPs were dried and dissolved in 13 mL of water to obtain ~10 mM (in terms of numbers of metal atoms) NP solutions. In the case of AuMUA, the pH of the solution was adjusted to ~11 with 0.2 M solution of NMe_4OH.

Preparation of a mixture of oppositely charged nanoparticles

Solution of TMA-coated NPs was titrated with ~100 μL aliquots of fully deprotonated (at pH = 11) MUA-coated NPs (note: titrating MUA particles with TMA

particles gave identical results, seeref. 17). As described in our earlier publications, the oppositely charged NPs precipitate at the point of electroneutrality, whereby the sum of charges on these particles is zero, $\sum Q_{NP(+)} + \sum Q_{NP(-)} = 0$. The precipitated NPs were collected, centrifuged and washed with DI water to remove excess salts. Finally, NPs were redissolved in DI water upon gentle heating. This solution was then stable for at least several months. For further details, see ref. 9, 16 and 17.

General procedure for crystallization of salts in the presence of NPs

In a typical experiment, 1 μmol (in terms of Au atoms) of the oppositely charged NPs was dissolved in 3 mL of water and DMSO (2 : 1 v/v).To this solution, either copper sulfate (n_{CuSO4} = 0.3–1.0 μmol) or nickel sulfate (n_{NiSO4} = 0.15–0.18 μmol) was added, the pH was adjusted to ~8 by addition of tetramethylammonium hydroxide, and then water (the "good" solvent) was evaporated slowly, over 16–24 h at $T = 65$ °C. In the last stages of evaporation, a dark brown solid precipitated from DMSO. This solid was washed several times with acetonitrile, deposited onto a TEM grid, dried under high vacuum, and then characterized by electron microscopy (TEM and SEM); composition scans were taken on a TEM equipped with an electron diffraction spectroscopy, EDS, detector. All nanoparticle assemblies characterized in this way were stable under organic solvent (DMSO) or in the air for at least several months.

3 Results and discussion

In our previous work on microcrystallization controlled by oppositely charged NPs, we delineated two main regimes: (1) one in which the salts are readily soluble and do not alter the crystallization of the NPs into all-nanoparticle crystals, and (2) one in which the salts are sparingly soluble such that their crystallization competes with the aggregation of the (+)/(–) NPs on the surfaces of the growing crystals, thereby limiting the crystals' growth. We rationalized both types of behaviors using a continuum description of the salt/NP systems and taking into account the interplay between salt solubility and Debye NP-NP screening effects (*i.e.*, crystallization of salt changes the screening length in the system and facilitates cooperative adsorption of the (+)/(–) NPs onto the growing salt microcrystals, for details, seeref. 24). The systems we study here illustrate that this description is only the first-order approximation and the mixtures of co-crystallizing (+)/(–) NPs and inorganic salts can produce a richer repertoire of nano- and microstructures whose morphologies depend strongly on the specific nature of salts used.

We consider $NiSO_4$ and $CuSO_4$ salts which share the same anion and their cations have the same valence. In this way, the Debye screening effects imparted by a given concentration of either of these salts are identical. We note that if it were predominantly the screening effects that control crystallization/assembly in the system, one could expect similar structures formed in the presence of $NiSO_4$ or $CuSO_4$. This, however, is not what we observed in experiments.

In the absence or at very low concentrations of Cu^{2+} or Ni^{2+} salts, the oppositely charged NPs formed regularly faceted, all-nanoparticle crystals such as those illustrated in Fig. 1 (*arrow to the left*) and described in our previous publications.[9,25,26] The effects of the salt on NP organization became significant only at higher concentrations and depended on the salt's nature.

For instance, for $NiSO_4$ at typical nanoparticle concentrations $C_{NP} \sim 0.33$ mM (n_{NP} = 1 μmol) and salt concentrations around $C_{NiSO4} = 0.05$ mM (n_{NiSO4} = 0.15 μmol), the NPs formed supraspherical (SS) aggregates (Fig. 1, *top right* panel and Fig. 2a,b). These supraspheres had average diameters ~250 nm and were relatively monodisperse (standard deviation in size ~20%). The compositional EDS scans over these structures evidenced clear gold and sulfur peaks but the concentrations of nickel were below the detection limit (Fig. 2b). The mechanism of formation

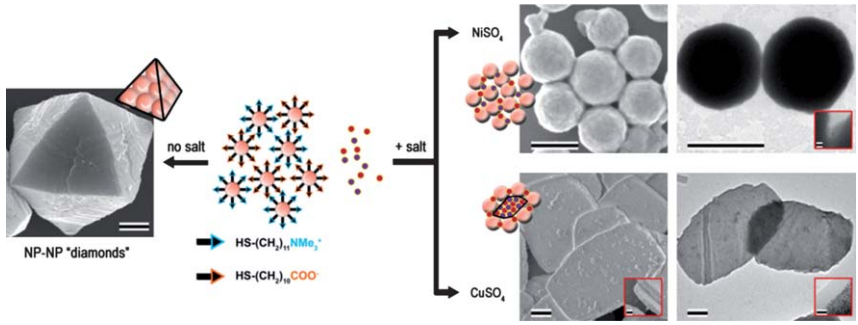

Fig. 1 Self-assembly of oppositely charged nanoparticles in the absence and in the presence of salts. In the absence or at low concentrations of either Ni^{2+} (C_{NiSO4} < 0.05 mM) or Cu^{2+} (C_{CuSO4} < 0.1 mM) salts (left), the positively and negatively charged nanoparticles nucleate and grow into all-nanoparticle crystals. At higher salt concentrations (right), the NPs form supraspheres (with $NiSO_4$, C_{NiSO4} > 0.05 mM) in which the MUA particles are "glued" by the salt cations, or plates (with $Cu(OH)_2/CuSO_4$ C_{CuSO4} > 0.1 mM) in which a nanoscopic needle-like crystals of $Cu(OH)_2$ act as templates onto which the NPs adsorb. Scale bars = 250 nm in all images, (150 nm in SEM inset and 25 nm in both TEM insets).

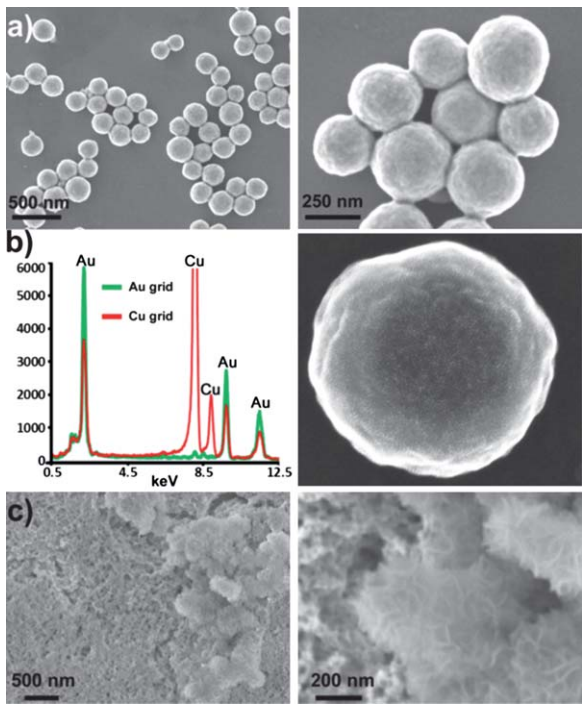

Fig. 2 (a) SEM images of supraspherical assemblies formed from the NPs in the presence of $NiSO_4$ (here, using $C_{NP} \sim 0.33$ mM, $n_{NP} = 1$ μmol, salt concentrations $C_{NiSO4} = 0.05$ mM, $n_{NiSO4} = 0.15$ μmol); (b) EDS spectra of a single suprasphere on copper and gold grids reveal the presence of gold (from nanoparticles) and not of any detectable amount of nickel. (c) Typical images of nickel hydroxide aggregates on top of structureless NP precipitates. Such structures form at high concentrations of $NiSO_4$ (C_{NiSO4} > 0.15 mM).

of similar supraspherical aggregates was studied in our earlier papers on nanoparticle assembly mediated by organic ligands.[27,28] Similar to these works, the NPs in our current system can aggregate due to the bridging of the carboxylate groups of

the MUA ligands by the Ni^{2+} cations. The energy of such bridges is on the order of few kT and, combined with the van der Waals attractions between NPs' metal cores, can overcome the electrostatic NP-NP repulsions.[15,22,29] The supraspheres then form most likely[27,28] by a nucleation-and-growth mechanism, in which the free MUA and TMA NPs initially nucleate into small, thermodynamically stable (unless smaller than a critical size) clusters that subsequently grow by the addition of single NPs until all NPs available are used. We note that this scenario is expected to be operative only at relatively weak net-attractive interactions. At higher salt concentrations, where the NP–NP attractions become stronger (due to screening effects), the NPs precipitate/flocculate into structureless aggregates. This is illustrated in Fig. 2c which shows NP precipitate with some microcrystals of nickel sulfate formed from an excess of salt in the last stages of water evaporation[30] (the "branched" structure of $NiSO_4$ microcrystals is indicative of diffusional limitations during the process).

The assemblies formed in the presence of copper sulfate ($n_{CuSO4} = 0.6$–2.0 μmol) were markedly different from those observed in $NiSO_4$ experiments (note: at higher salt concentrations, the NPs gradually precipitated). At $n_{CuSO4} = 2.0$ μmol, these structures were relatively monodisperse thin plates (up to ~2 μm wide, ~4 μm long and 100–150 nm thick, Fig. 3a). Decreasing the amount of copper salt to $n_{CuSO4} = 1.4$ μmol led to the formation of square, submicron plates (~0.5 μm × ~0.5 μm × 50 nm, Fig. 3b). Upon further decrease of the n_{CuSO4} to 1.0 μmol, needle-like structures formed (~200 nm × 50 nm × 20 nm, Fig. 3c) and at $n_{CuSO4} =$ 0.6 μmol, the assemblies had a morphology of needles/sheets only ~10 nm thick

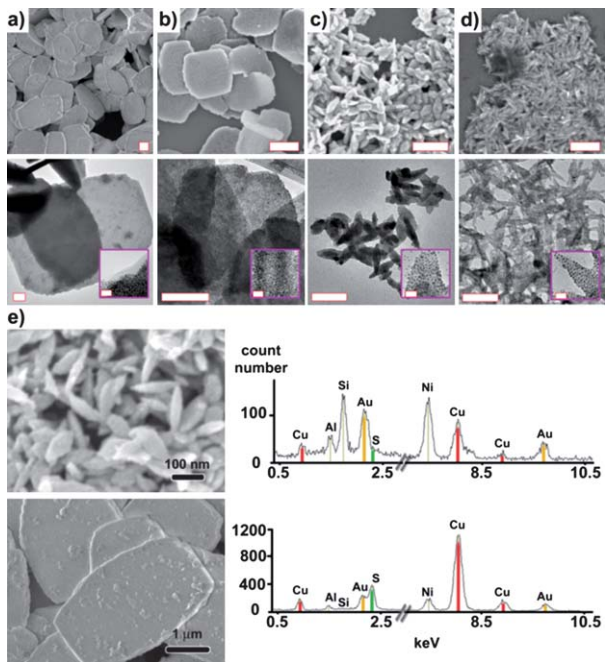

Fig. 3 (a–d) SEM (top row) and TEM (bottom row) images showing size- and shape dependent self-assembly of oppositely charged nanoparticles mediated by Cu^{2+}. The assemblies (a)–(d) correspond to the amounts of $CuSO_4$ 2.0, 1.4, 1.0 and 0.6 μmol, respectively. All scalebars correspond to 500 nm in the SEM images, 200 nm in the TEM images, and 25 nm in the insets. (e) EDS spectra of smaller "needles" (top) from Fig. 3d, and larger "plates" (bottom) depicted in Fig. 3a, grown from copper sulfate and oppositely charged NPs. The lower ratio of intensities of the S:Au peaks in the top image and the higher ratio of the same peaks in the bottom image suggest that small "needles" are composed predominantly of NP-coated copper hydroxide, while large plates contain extra NP layers "glued" together by copper sulfate.

(typical dimensions, ~200 nm × 30 nm × 10 nm, Fig. 3d). The compositional scans of these structures (Fig. 3e) feature prominent peaks corresponding to copper (from salt) and gold (from NPs). Interestingly, in the case of thin needles or sheets (Fig. 3c,d), the sulfur peak is weak compared to the gold peaks, while for the large microplates (Fig. 3a, b), the opposite is true.

The marked differences in the morphologies of structures formed using $NiSO_4$ and $CuSO_4$ can be rationalized by the difference in solubilities of the nickel and copper salts. Specifically, $NiSO_4$ is highly soluble ($K_{SP} = 25$ M^2) and does not precipitate/crystallize during self-assembly of the NPs into supraspheres—as discussed above, the major role of the salt in the system is to form bridges between MUA particles. The mechanism of the self-assembly becomes more complex with $CuSO_4$. While this salt is, in itself, readily soluble, an equilibrium between $CuSO_4$ and poorly soluble $Cu(OH)_2$ is established at basic pH values such as those we used here. The key phenomenon during our SA experiments is therefore that copper hydroxide can crystallize first to form small "seeds" onto which the NPs adsorb. To support this hypothesis, we performed a series of experiments where the amount of TMAOH was kept constant, $n_{base} = 1.6$ μmol, while the amounts of copper sulfate varied, $n_{CuSO4} = 0.6$, 1.0, 1.4, and 2 μmol. At the lowest concentration of copper sulfate, all salt reacted with an excess of base and formed copper hydroxide, which crystallized in the form of thin sheets covered with only a thin film of the NPs (similar to Fig. 3d and Fig. 4a). The EDS spectra evidenced that the ratio of intensities of the sulfur and gold peaks was low. Importantly, its value agreed with the expected ratio of sulfur in the thiolate SAMs to the gold in the NP cores—in other words, the only source of sulfur peaks was from the SAMs and there was no excess sulfur present from $CuSO_4$. When concentration of $CuSO_4$ was increased, not all of it reacted with the base and the proportion of unreacted $CuSO_4$ to the $Cu(OH)_2$ "seeds" increased. As a result, more Cu^{2+} cations remained in solution and were able to bridge[29] more NPs adsorbing onto the $Cu(OH)_2$ seeds (with the SO_4^{2-} counterions contributing to the increased intensity of the EDS sulfur peaks). Consequently,

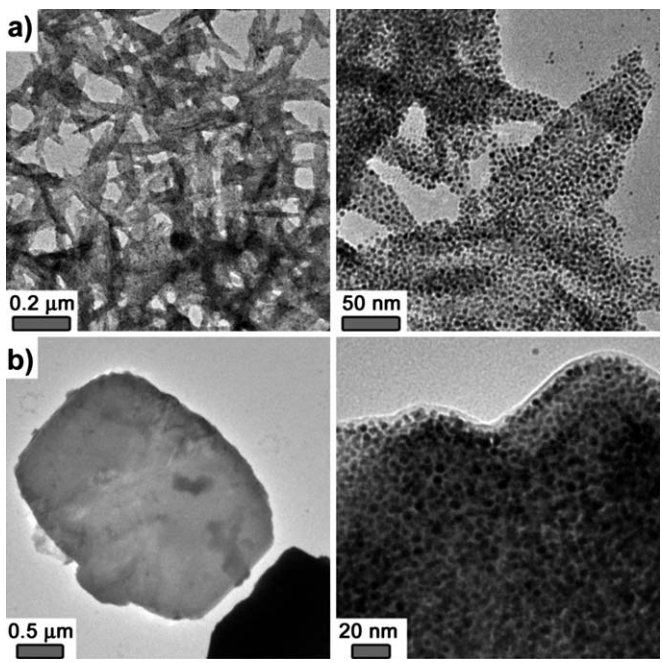

Fig. 4 TEM images of $Cu(OH)_2$ structures coated with (+)/(–) nanoparticles: (a) thin sheets coated with NP monolayers; (b) nanoplates coated with multiple layers of NPs.

the assemblies grew into larger nanoplates covered with multiple layers of nanoparticles. The formation of NP multilayers was confirmed by TEM imaging (Fig. 3a and Fig. 4b) and the presence of copper sulfate on the copper hydroxide "seeds" was evidenced by an increased intensity of sulfur and copper peaks relative to gold, as measured by the EDS, Fig. 3e.

It is interesting to compare and contrast our NP/Cu^{2+} structures with copper hydroxide[31] and copper oxide[32] microstructures prepared by other groups *via* surfactant-assisted, shape-dependent syntheses. In particular, copper hydroxide microplates with shapes similar to those we obtained were recently reported[31] *via* a procedure involving copper chloride in the presence of bis-(amidoethyl-carbamoylethyl) octadecylamine as a surfactant and ammonium chloride as a shape modifying agent. Interestingly, when this experiment was performed in the absence of surfactant, spherical $Cu(OH)_2$ nanoparticles (~10 nm in diameter) were obtained, which then grew into irregularly-shaped particles several hundreds of nanometers large. In this context, our current results suggest that oppositely charged nanoparticles can act analogously to organic surfactants by stabilizing crystalline nuclei and modulating the growth of microcrystals. The key difference, however, between small-molecule surfactants and our NPs is that the latter benefit from the polyvalent nature of interactions between the crystals and the multiple ligands immobilized onto the NPs—if these ligands (or their structural analogues) are not tethered onto nanoparticles and are free in solution, they are not capable of regulating the growth of crystals studied here or in our previous paper.[24] This is so because adsorption of individual surfactants onto a surface of a growing microcrystal is entropically unfavorable, with penalty for the translational degrees of freedom of each adsorbed species approximately $kT\ln(Ad/V)$, where A is the total area available to the adsorbate, d is the size of the adsorbate, and V is the solution volume. Consequently, interactions between the adsorbing molecules and the crystal surface must be sufficiently strong to yield an overall favorable/negative free energy of adsorption. In contrast, the entropic penalty is minimal for ligands already preorganized on the NPs. Even though the MUA or TMA ligands are, individually, not necessarily strong and specific binders to salt crystals, their large numbers on the NPs act in concert and add up to appreciable free energies of adsorption onto various surfaces (not only crystals but also glasses, polymers or even metals, for details, seeref. 18 and 33). This process is further aided by the electrostatic attractions between the (+) and the (–) NPs.[34]

Naturally, it would be desirable to extend the NP-surfactant methods to systems that are not necessarily based on charge–charge interactions and to organic microcrystals. In doing so, the attractive NP(+)/NP(–) interactions need to be replaced by other types of interactions capable of harboring the NPs onto the crystals. While the search for such systems is only in its preliminary stages, we have been able to demonstrate the proof-of-the-concept experiments using nanoparticles covered with 1,6-difluoro-4-mercaptophenol (DFMP) ligands (Fig. 5a) and donor–acceptor organic crystals composed of 1,5-bis[2-(2-hydroxyethoxy)ethoxy]naphthalene (donor, D) and pyromellitic diimide (acceptor, A) (Fig. 5b, details on the synthesis and properties of such crystals will be published separately). These molecules form D–A stacks along the crystal, exposing EG-chains and imide groups on the crystal's surface. We designed the SAMs on the NPs in such a way that adsorption of particles onto the D–A crystals would occur through the formation of hydrogen bonds between phenol moieties on the NPs' surfaces and both the EG units and the carbonyl oxygens of the donor and acceptor molecules, respectively. At the same time, the relatively small thickness of the DFMP SAMs on the NP surfaces (~0.6 nm) was beneficial since it translated into strong attractive interactions between the particles (mostly due to van der Waals attractions between the Au cores[15])—this allowed for dense packing of NPs on the surfaces of the organic crystals. The images in Fig. 5c and 5d illustrate the NP coatings formed on both macroscopic as well as microscopic donor–acceptor crystals.

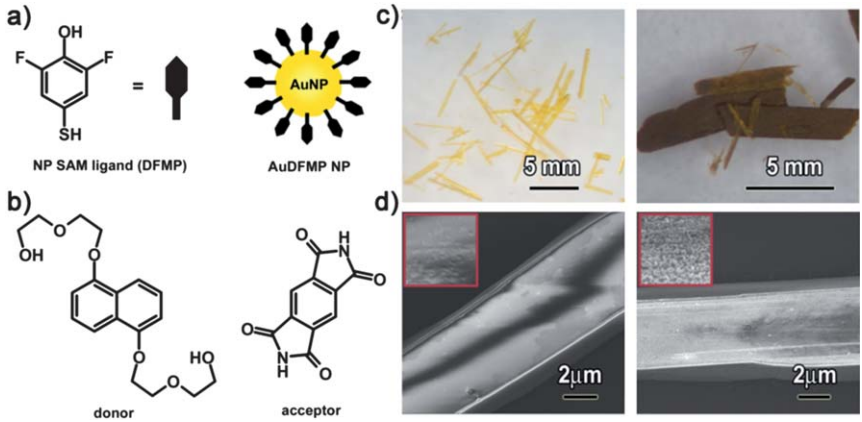

Fig. 5 Structures of (a) 2,6-difluoro-4-mercaptophenol, DFMP, used to form SAMs on AuNPs. (b) Molecules crystallizing into donor–acceptor organic crystals. (c) Optical and (d) SEM images of D–A crystals before (left) and after (right) coating them with AuDFMP NPs.

In summary, we demonstrated a cation-selective self-assembly of oppositely charged nanoparticles as well as first experiments with NP coated organic crystals. One unique feature of these systems is that the ligands on the NPs can interact with the crystals polyvalently—in this way, even weakly binding ligands can turn the NPs into strongly binding crystal-growth modifiers. In the case of nESA, these effects are supplemented by cation-bridging interactions which further enrich the repertoire of composite structures that can be prepared by co-crystallizing salts and nanoparticles. One appealing avenue for future research might be to combine the catalytic properties of the crystalline nanoseeds (*e.g.*, $Cu(OH)_2$ catalyzes oxidation of phenols by hydrogen peroxide[31]) with the selective substrate permeability[35] of the NPs coating these seeds.

References

1 D. L. Feldheim and C. D. Keating, *Chem. Soc. Rev.*, 1998, **27**, 1–12.
2 S. J. Oldenburg, R. D. Averitt, S. L. Westcott and N. J. Halas, *Chem. Phys. Lett.*, 1998, **288**, 243–247.
3 S. H. Sun, *Adv. Mater.*, 2006, **18**, 393–403.
4 H. Zeng, J. Li, J. P. Liu, Z. L. Wang and S. H. Sun, *Nature*, 2002, **420**, 395–398.
5 J. H. Fendler, *Chem. Mater.*, 2001, **13**, 3196–3210.
6 L. S. Zhong, J. S. Hu, H. P. Liang, A. M. Cao, W. G. Song and L. J. Wan, *Adv. Mater.*, 2006, **18**, 2426.
7 J. M. Perez, L. Josephson, T. O'Loughlin, D. Hogemann and R. Weissleder, *Nature Biotechnology*, 2002, **20**, 816–820.
8 A. M. Cao, J. S. Hu, H. P. Liang and L. J. Wan, *Angew. Chem., Int. Ed.*, 2005, **44**, 4391–4395.
9 A. M. Kalsin, M. Fialkowski, M. Paszewski, S. K. Smoukov, K. J. M. Bishop and B. A. Grzybowski, *Science*, 2006, **312**, 420–424.
10 Z. Y. Tang, Z. L. Zhang, Y. Wang, S. C. Glotzer and N. A. Kotov, *Science*, 2006, **314**, 274–278.
11 S. Srivastava, A. Santos, K. Critchley, K. S. Kim, P. Podsiadlo, K. Sun, J. Lee, C. L. Xu, G. D. Lilly, S. C. Glotzer and N. A. Kotov, *Science*, 2010, **327**, 1355–1359.
12 Y. H. Wei, K. J. M. Bishop, J. Kim, S. Soh and B. A. Grzybowski, *Angew. Chem., Int. Ed.*, 2009, **48**, 9477–9480.
13 M. A. Olson, A. Coskun, R. Klajn, L. Fang, S. K. Dey, K. P. Browne, B. A. Grzybowski and J. F. Stoddart, *Nano Lett.*, 2009, **9**, 3185–3190.
14 K. Liu, Z. H. Nie, N. N. Zhao, W. Li, M. Rubinstein and E. Kumacheva, *Science*, 2010, **329**, 197–200.
15 K. J. M. Bishop, C. E. Wilmer, S. Soh and B. A. Grzybowski, *Small*, 2009, **5**, 1600–1630.

16 A. M. Kalsin, B. Kowalczyk, P. Wesson, M. Paszewski and B. A. Grzybowski, *J. Am. Chem. Soc.*, 2007, **129**, 6664.
17 A. M. Kalsin, B. Kowalczyk, S. K. Smoukov, R. Klajn and B. A. Grzybowski, *J. Am. Chem. Soc.*, 2006, **128**, 15046–15047.
18 S. K. Smoukov, K. J. M. Bishop, B. Kowalczyk, A. M. Kalsin and B. A. Grzybowski, *J. Am. Chem. Soc.*, 2007, **129**, 15623–15630.
19 D. A. Walker, K. P. Browne, B. Kowalczyk and B. A. Grzybowski, *Angew. Chem., Int. Ed.*, 2010, **49**, 6760–6763.
20 D. A. Walker, C. E. Wilmer, B. Kowalczyk, K. J. M. Bishop and B. A. Grzybowski, *Nano Lett.*, 2010, **10**, 2275–2280.
21 I. Lagzi, B. Kowalczyk, D. W. Wang and B. A. Grzybowski, *Angew. Chem., Int. Ed.*, 2010, **49**, 8616–8619.
22 D. A. Walker, B. Kowalczyk, M. O. de la Cruz and B. A. Grzybowski, *Nanoscale*, 2011, **3**, 1316–1344.
23 D. Witt, R. Klajn, P. Barski and B. A. Grzybowski, *Curr. Org. Chem.*, 2004, **8**, 1763–1797.
24 B. Kowalczyk, K. J. M. Bishop, I. Lagzi, D. W. Wang, Y. H. Wei, S. B. Han and B. A. Grzybowski, *Nat. Mater.*, 2012, **11**, 227–232.
25 A. M. Kalsin and B. A. Grzybowski, *Nano Lett.*, 2007, **7**, 1018–1021.
26 B. Kowalczyk, A. M. Kalsin, R. Orlik, K. J. M. Bishop, A. Z. Patashinskii, A. Mitus and B. A. Grzybowski, *Chem.–Eur. J.*, 2009, **15**, 2032–2035.
27 R. Klajn, K. J. M. Bishop, M. Fialkowski, M. Paszewski, C. J. Campbell, T. P. Gray and B. A. Grzybowski, *Science*, 2007, **316**, 261–264.
28 R. Klajn, K. J. M. Bishop and B. A. Grzybowski, *Proc. Natl. Acad. Sci. U. S. A.*, 2007, **104**, 10305–10309.
29 D. W. Wang, B. Tejerina, I. Lagzi, B. Kowalczyk and B. A. Grzybowski, *ACS Nano*, 2011, **5**, 530–536.
30 When the pH of NP-salt mixture was raised above ~8 by addition of TMAOH flower-like $Ni(OH)_2$ microcrystals and NPs formed separately and precipitated (see Fig. 2c). Since the solubility of $Ni(OH)_2$ is 2–3 orders of magnitude higher than that of copper hydroxide (pK_{SO} $Ni(OH)_2 = 17.2$, pK_{SO} $Cu(OH)_2 = 19.7$), nickel salts can be stable in solution for longer times during crystallization, screening the interactions between NPs and causing random precipitation of NPs. The excess of salt precipitates toward the end of the evaporation in the form of "wavy" flower-like microstructures.
31 G. H. Lin, W. F. Jia, W. S. Lu and L. Jiang, *J. Colloid Interface Sci.*, 2011, **353**, 392–397.
32 X. D. Liang, L. Gao, S. W. Yang and J. Sun, *Adv. Mater.*, 2009, **21**, 2068–2071.
33 S. Huda, S. K. Smoukov, H. Nakanishi, B. Kowalczyk, K. Bishop and B. A. Grzybowski, *ACS Appl. Mater. Interfaces*, 2010, **2**, 1206–1210.
34 K. V. Tretiakov, K. J. M. Bishop, B. Kowalczyk, A. Jaiswal, M. A. Poggi and B. A. Grzybowski, *J. Phys. Chem. A*, 2009, **113**, 3799–3803.
35 B. Kowalczyk, I. Lagzi and B. A. Grzybowski, *Nanoscale*, 2010, **2**, 2366–2369.